Electric Field Perturbations of Spiral Waves Attached to Millimeter-Size Obstacles

Joshua Cysyk and Leslie Tung
Department of Biomedical Engineering, The Johns Hopkins University, Baltimore, Maryland

ABSTRACT Reentrant spiral waves can become pinned to small anatomical obstacles in the heart and lead to monomorphic ventricular tachycardia that can degenerate into polymorphic tachycardia and ventricular fibrillation. Electric field-induced secondary source stimulation can excite directly at the obstacle, and may provide a means to terminate the pinned wave or inhibit the transition to more complex arrhythmia. We used confluent monolayers of neonatal rat ventricular myocytes to investigate the use of low intensity electric field stimulation to perturb the spiral wave. A hole 2–4 mm in diameter was created in the center to pin the spiral wave. Monolayers were stained with voltage-sensitive dye di-4-ANEPPS and mapped at 253 sites. Spiral waves were initiated that attached to the hole ($n = 10$ monolayers). Electric field pulses 1-s in duration were delivered with increasing strength (0.5–5 V/cm) until the wave terminated after detaching from the hole. At subdetachment intensities, cycle length increased with field strength, was sustained for the duration of the pulse, and returned to its original value after termination of the pulse. Mechanistically, conduction velocity near the wave tip decreased with field strength in the region of depolarization at the obstacle. In summary, electric fields cause strength-dependent slowing or detachment of pinned spiral waves. Our results suggest a means to decelerate tachycardia that may help to prevent wave degeneration.

INTRODUCTION

Monomorphic ventricular tachycardia can result from functional spiral waves that are anchored (pinned) to some anatomical heterogeneity. The breakup of a spiral wave can lead to ventricular fibrillation and sudden cardiac death (1–3). The only effective treatment to terminate fibrillation is with high-energy electrical shocks. These defibrillation shocks can have adverse side effects on the integrity and function of the myocardium (4) and can cause psychological trauma (5). It would be of great therapeutic value to limit the use of defibrillation shocks by terminating tachycardia before degeneration of ventricular tachycardia to ventricular fibrillation can occur.

Antitachycardia pacing is used to entrain and terminate the underlying reentrant wave via low energy pacing from an implantable device. The pacing success depends, in part, on the proximity of the implanted electrodes to the core of the wave (6). Although placement of the electrodes at the core generally is not possible, stimulation near the core may be feasible by using electric fields (7).

Direct activation of cardiac tissue has been observed with pulsed electric fields and attributed to secondary source stimulation (8). These secondary sources occur at tissue inhomogeneities (9) and have been characterized using the bidomain model as distinct from sources at the physical field electrodes (10). It has been shown experimentally that the strength of the secondary sources increases with electric field strength (11). For a spiral wave pinned to an anatomical obstacle, secondary sources can be utilized to deliver a pulse near the tip of the wavefront, and if properly timed can cause the wave to unpin (7,12).

The goal of this study was to use electric field stimulation to modulate the dynamics of a spiral wave pinned to an obstacle in a cardiac monolayer. Our hypothesis is that the secondary sources formed at an obstacle during the electric field pulse can interact with the pinned wave in different ways at pulse-make, at pulse-break, or throughout the duration of the pulse. The interactions can take the form of advancement, unpinning, slowing, or acceleration of the pinned wave.

METHODS

Cell culture

Neonatal rat ventricular myocytes were dissociated from ventricles of two-day-old Sprague-Dawley rats (Harlan; Indianapolis, IN), as previously described (13). Cells were plated (using 10^6 cells) on 22-mm diameter plastic coverslips previously coated with 25 μg/ml fibronectin (Sigma, St. Louis, MO). Holes of 3–4 mm diameter were drilled into the coverslips before fibronectin coating. Experiments were performed on days 6–9 after plating.

Electrophysiological recording

Transmembrane voltage was recorded using the method of contact fluorescence imaging (14). Monolayer preparations were visually inspected under a microscope before mapping. Only confluent, beating monolayers were selected for experiments. Cells were stained with 10 μM di-4-ANEPPS and continually superfused with warmed (35 $\pm$ 1°C) Tyrode's solution (135 mM NaCl, 5.4 mM KCl, 1.8 mM $CaCl_2$, 1.0 mM $MgCl_2$, 0.33 mM NaH_2PO_4, 5.0 mM HEPES, and 5.0 mM glucose).

Monolayer preparations were placed in an experimental chamber and imaged over 253 1-mm-diameter sites arranged in a 17-mm-diameter hexagonal array. The array is centered under the 22-mm-diameter coverslip, and additional cultured cells lie outside of the field of view. The details of the experimental setup have been reported previously (14,15).

Submitted June 26, 2007, and accepted for publication September 26, 2007.

Address reprint requests to Leslie Tung, Tel.: 410-955-7453; E-mail: ltung@jhu.edu.

Editor: David A. Eisner.

0006-3495/08/02/1533/09 $2.00

doi: 10.1529/biophysj.107.116244

Electric field stimulation was applied using constant voltage stimulation across a parallel set of platinum wire electrodes 2.5-cm-long placed in the bath outside of the monolayer preparation on either side. The field intensity was calibrated for a given current from the peak voltage across AgCl reference electrodes at a 1-cm separation in the chamber.

Experimental protocol

To induce reentry, stimulation from a bipolar line electrode (S1) was followed by stimulation from a bipolar area electrode (S2) with a coupling interval long enough for the monolayer to be captured by both stimuli (15). The coupling interval was gradually reduced until the S2 stimulus fell in the vulnerable window, generating reentry. In some cases, rapid point pacing was used. Stimulation was delivered at increasing frequencies until 2:1 block occurred or reentry was generated. Stable reentry was considered to be successfully induced if the wave pinned to the obstacle and remained pinned for at least 1 min. After reentry initiation, a 1-s field stimulus pulse was delivered to the monolayer at an intensity between 0.5 and 1.0 V/cm. The stimulus intensity was increased with repeated pulses (1 min delay between trials) until reentry terminated (typically at 3–4 V/cm).

Data analysis

For the duration of the optical recording (2–4 s), the fluorescence signal baseline decreased because of heating of the LED lamp and photobleaching of the fluorescent dye. Baseline drift was corrected for by subtraction of a third-order polynomial from the optical signal at each recording site. The voltage maps were standardized to give a clockwise-rotating wave with a positive polarity field directed from top to bottom. Isopotential maps were generated by interpolation over a grid with 0.1-mm step size. Wavefronts were defined from isochronal lines interpolated from the AP upstroke at each recording site. After stimulation, detachment of the wave tip from the obstacle was determined by visual inspection. A point 2-mm from the wave tip and on the wavefront was used to define the angle of the wave at stimulation. Conduction velocity was defined as the inverse of the distance along a line normal to the wavefront that crossed isochrones spaced 10 ms apart. Cycle length and conduction velocity measurements during field stimulation were averaged over the interval from 200 ms after pulse-make to the end of the 1-s pulse.

RESULTS

Reentry was initiated in 10 monolayer preparations containing a single obstacle 2 to 4 mm in diameter that provided a site for pinning. The reentry cycle length (CL) was stable for each experiment, but varied between monolayers. For all monolayers, the average CL was 133 ms, and ranged between 108 ms and 178 ms. There was no dependence of CL on hole size ($R^2 < 0.01$). After initiation, one-second electric field pulses were delivered, and the interaction of the field with the pinned spiral wave was mapped optically. The intensity of the pulse was increased until the wave terminated. Positive or negative pulses were used, and the results were independent of pulse polarity after accounting for a 180° rotational phase shift of the wave.

The effect of the 1-s electric field pulse can be divided into three regimes: pulse make, pulse duration, and pulse break. At pulse make, stimulation can occur that interacts with the pinned wave and affects the wave dynamics for the following cycle. For the remaining duration of the pulse, the wave propagates through a constant electric field. At the end of the pulse, pulse break stimulation can occur and interact with the pinned wave as well. The effects of each part of the field pulse were considered separately.

Pulse-make stimulation

An electric field across a homogenous monolayer with an obstacle will theoretically create a region of depolarization at the obstacle, providing a secondary source site for stimulation. Fig. 1 *A* shows the voltage maps from a 1-s duration, 0.9 V/cm field pulse applied across a quiescent monolayer containing a 2.6-mm-diameter obstacle. The electric field is oriented from top to bottom, and pulse-make stimulation occurred at the top side of the obstacle corresponding to the depolarized region. Stimulation spread around and out from the obstacle. In some cases (not shown in Fig. 1 *A*) stimulation occurred at both the edge of the monolayer at the field cathode and at the obstacle.

When a pinned spiral wave was present, secondary source stimulation timed to be in front of the pinned wave at pulse-make created a pair of oppositely propagating waves at the obstacle (Fig. 1 *B*, $t = 10$ ms). The counterclockwise wave detached the spiral wave from the obstacle, while the clockwise wave continued unimpeded and remained pinned to the obstacle ($t = 30$ ms). The net effect was advancement of the original pinned spiral wave. Fig. 1 *C* shows the same pinned wave with a stronger field stimulus again timed so that excitation occurred at the same location in front of the wave. This time, the stimulation was strong enough to cause the wave to advance and detach from the hole ($t = 60$ ms). At $t = 100$ ms, the wave was able to pivot enough around the obstacle, reattach to the bottom side and continue its rotation (not shown). An even larger stimulus with the same timing as in Fig. 1, *B* and *C*, advanced the wave, as shown in Fig. 1 *D*. As before, the wave advanced around the obstacle and detached. However, this time as the wave began to turn it was unable to reattach ($t = 80$ ms), and then drifted to the boundary and terminated.

Out of 128 stimuli (0.5 to 4.5 V/cm) delivered with random timing across 10 monolayers, 47 detached the wave (37%). In 38 of the 47 cases (81%), the wave was able to reattach to the obstacle. In one case, the wave reattached to a different location in the monolayer. All pulse-make detachment events occurred on the first cycle of the wave after stimulation.

To quantify these results further, the position of the wave at the time of stimulation was defined as the angle between the stimulation site and wavefront at the time of stimulation (Fig. 2 *A*). All wave angles were standardized in terms of a wave rotating clockwise with a positive field pulse directed from top to bottom; therefore, the region of depolarization was centered at 0°, and the region of hyperpolarization at 180°. The dependence of detachment and termination on wave position at stimulus pulse-make is shown in Fig. 2 *B* as a function of field intensity. The probability of detachment

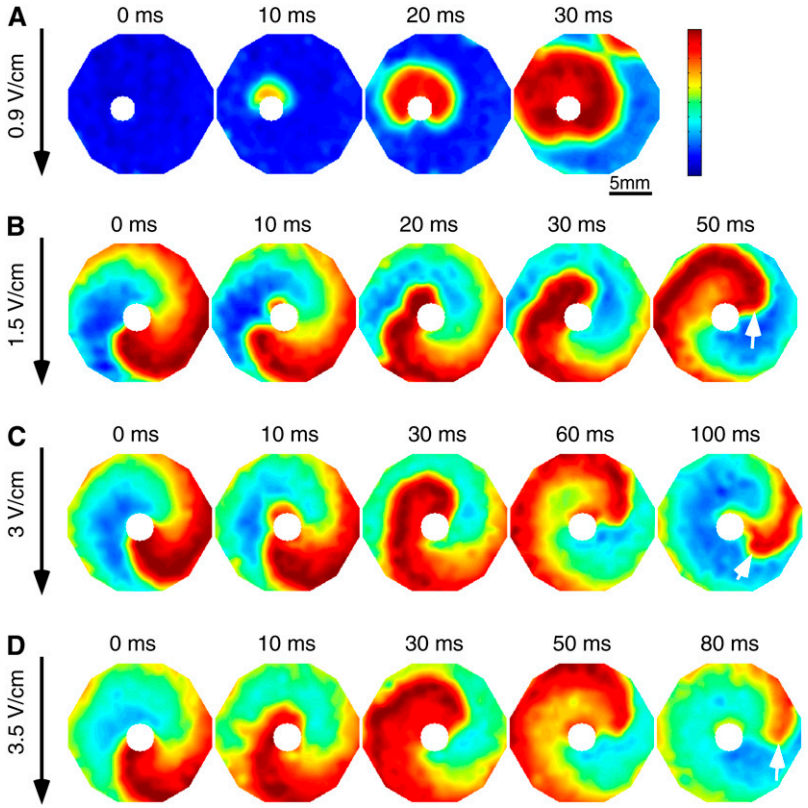

FIGURE 1 Optical maps of wave propagation in cardiac cell monolayers. (*A*) 0.9 V/cm electric field stimulation across quiescent monolayer with 2.6-mm-diameter obstacle. (*B–D*) Stimulation at obstacle (3 mm diameter) in front of the pinned wave caused the wave to advance or partially detach. (*B*) 1.5 V/cm field stimulus caused the wave to advance and remain pinned to the obstacle. (*C*) 3 V/cm field stimulus advanced the wave and caused the wave to detach, but the wave was able to reattach during the same cycle. (*D*) 3.5 V/cm field stimulus advanced and unpinned the wave, and the wave drifted to the boundary and terminated. In all maps the electric field is oriented from top to bottom, and the depolarized region is located on the top side of the obstacle depicted by the white circle. The field stimulus was turned on at $t = 0$ ms and remained on for 1-s. White arrows show differing degrees of detachment of the wave tip from the obstacle. The color bar indicates the normalized transmembrane voltage: blue represents the resting state, and red represents the peak of the action potential.

increased with field intensity: only one pulse with intensity <2 V/cm detached the wave. The likelihood of wave termination after detachment increased with field intensity as well. Across all experiments, there was no optimal wave position for detachment or termination. The mean angle of detachment was 171° (2.98 rad) with a concentration, $r = 0.06$, which was not significantly different from a circular distribution using the Rayleigh Z test ($p = 0.84$).

Waves pinned to smaller obstacles tended to detach more often during field stimulation. At field strengths ≤2 V/cm, 14% of pulses detached waves attached to 2-mm-diameter holes ($n = 29$), whereas only 6% of pulses detached waves pinned to 3–4 mm-diameter holes ($n = 24$). At field strengths between 2 and 3 V/cm, 67% and 50% of stimuli detached waves pinned to 2 mm ($n = 9$) and 3–4 mm ($n = 22$) diameter holes, respectively. Wave termination occurred in 33% of the detachment events for 2-mm-diameter holes ($n = 12$), and 14% for 3–4-mm-diameter holes ($n = 28$). Waves that did not terminate after detachment were able to re-pin to the obstacle after one rotation.

Slowing during the pulse

After pulse-make, waves that remained pinned to the obstacle were subject to a constant electric field for multiple cycles of the wave. Fig. 3 shows a series of voltage maps of a

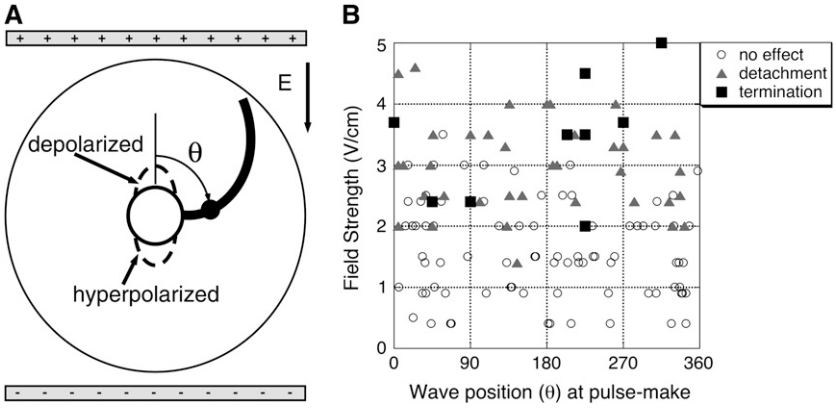

FIGURE 2 Effect of stimulus pulse-make on pinned spiral wave. (*A*) Wave-angle definition and field electrode arrangement across monolayer. For each experiment, depending on the direction of the field and chirality of the spiral wave, coordinates and angles were defined in such a way as to give a standardized clockwise-rotating wave with a positive polarity field directed from top to bottom, so that the region of depolarization would be at 0° and the region of hyperpolarization at 180°. The wave angle was measured between the stimulation site and a point along the wavefront 2 mm from the wave tip (*black circle*). (*B*) Field strength and timing dependence of wave detachment. Angle of the wavefront at time of pulse-make is shown. Total of 128 pulse-make trials across 10 monolayers are plotted, including 47 detachment events (37%).

wave pinned to the obstacle before, during, and after the electric field pulse (see Supplementary Materials, Movie 1). The voltage maps during the pulse were taken after the transients caused at pulse-make had subsided. Wave slowing during the field pulse can be seen by tracking the wavefront propagation in the voltage maps. In the first column, the wavefronts in all three panels are at the same position, but after 120 ms (*last column*) the wavefront during the field pulse lags behind the wavefronts before and after the field pulse (*white arrows*). Consistent with wave slowing, the wavelength of the pinned wave (thickness of *red region* in voltage map) was shorter during the electric field. After the electric field terminated, the frequency and wavelength of the pinned wave returned to their prepulse values. There were no instances of wave termination during the field pulse.

Action potential recordings from single sites around the obstacle are shown in Fig. 4 before, during, and after a 3 V/cm electric field pulse. The voltage map was constructed from the baseline shift in the action potentials at each recording site averaged over the interval from 200 ms after pulse-make to the end of the 1-s pulse. The field caused depolarization of the action potential baseline at sites within 2 mm of the top side of the obstacle. On the opposite side of the obstacle, hyperpolarization of the baseline was observed with a maximum effect near the obstacle. No significant baseline shift was observed on the sides of the obstacle.

Action potential recordings from single sites within the regions of depolarization and hyperpolarization are shown in more detail in Fig. 5 before, during, and after 3 V/cm stimulation. In addition to the elevated baseline in the region

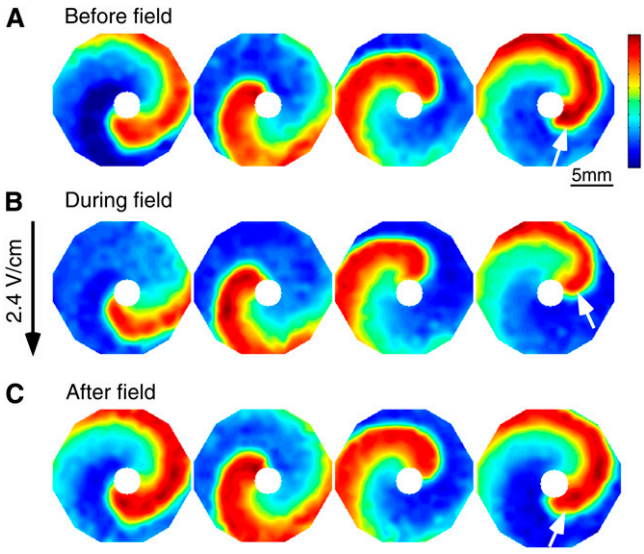

FIGURE 3 Voltage maps of a spiral wave pinned to a 3-mm obstacle during field stimulation. (*A*) Before electric field. (*B*) During 2.4 V/cm field applied from top to bottom. (*C*) After electric field. In each row, voltage maps are shown in 40-ms increments and white arrows in the final frame show position of the wave tip 120 ms after the initial frame. The color bar indicates the normalized transmembrane voltage: blue represents the resting state, and red represents the peak of the action potential.

of depolarization (top of obstacle) during stimulation, there was a reduction in the amplitude and maximum upstroke velocity of the action potential. At 3 V/cm field stimulation, the average normalized upstroke velocity of action potentials in the depolarized region ($n = 10$ monolayers) was 0.86 ± 0.12, which was statistically significant compared with 1 ($p < 0.005$). In the region of hyperpolarization (bottom of obstacle) there was a downward shift in the baseline, a reduction in the amplitude, and a slight increase in the maximum upstroke velocity of the action potential. At 3 V/cm field stimulation, the average normalized upstroke velocity of action potentials in the hyperpolarized region ($n = 10$ monolayers) was 1.02 ± 0.11. An increase in CL during the field pulse is evident in the action potential traces from both regions.

A representative plot of CL measured at the top of the obstacle during stimulation is shown in Fig. 6 *A*. At pulse-make, the wave advanced owing to stimulation at the obstacle, so that CL decreased. For the following cycle, CL increased and then remained elevated for the remainder of the pulse. After pulse-break, CL decreased below its prestimulus value before slowly returning to that value. The increase in CL of the pinned wave during the 1-s electric field pulse occurred in all monolayers tested. The dip and overshoot of CL at pulse-make did not occur in all experiments and depended on the wave position at the time of pulse-make.

For each set of trials applied to a given monolayer, CL increased monotonically with field strength. There was no dependence on field polarity, only on the magnitude of the field. In Fig. 6 *B*, CL during field stimulation is shown for all monolayers tested, and varied linearly with field strength. CL increased by 7% per V/cm for waves pinned to 2-mm-diameter obstacles ($R = 0.76$, $n = 2$), and by 13% per V/cm for waves pinned to 2.6 mm ($R = 0.95$, $n = 1$), 3 mm ($R = 0.83$, $n = 5$), and 4 mm ($R = 0.98$, $n = 2$) diameter obstacles.

Next, the manner of wavefront slowing during the field pulse was studied in greater detail. Fig. 7 *A* compares the propagation delay of the wave during field stimulation as it passed through the four quadrants surrounding the obstacle. The greatest propagation delay occurred as the wave propagated across the top of the obstacle (region of depolarization) and around toward the bottom of the obstacle. This delay increased with field intensity. There was no delay across the bottom of the obstacle (region of hyperpolarization) at 1 and 2 V/cm field intensities, but at 3 V/cm it could be seen. As the wave passed from the bottom of the obstacle toward the top there was no significant delay for the intensities tested.

Upon pulse-break, the propagation delays did not immediately cease but adopted a new pattern as shown in Fig. 7 *B*. The wave propagation across the top of the obstacle and around toward the bottom returned immediately to its prestimulus times. As the wave traveled across the bottom of the obstacle through the region that was hyperpolarized by the field pulse, the propagation time decreased (i.e., wave traveled faster). With increasing field intensity the propagation time decreased further. There was a modest decrease in the propagation time

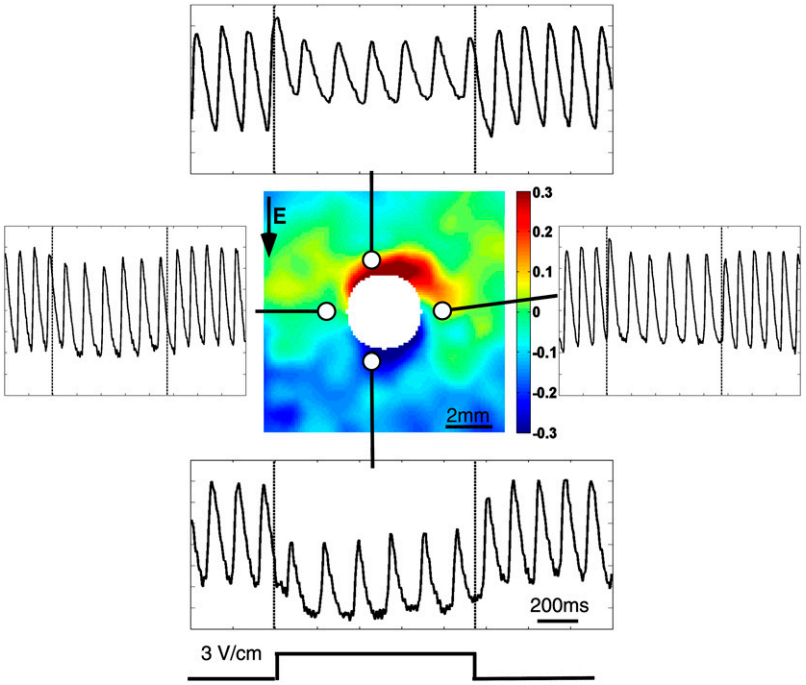

FIGURE 4 Polarization changes produced by the 3 V/cm electric field. A wave was pinned to a 3-mm obstacle, and a 1-s-long field pulse was applied from top to bottom across the monolayer. Action potential recordings are shown from four channels around the obstacle before, during, and after the field pulse. Dashed vertical lines indicate turn-on and turn-off of field pulse. Baseline change was measured from all channels during the pulse to create a polarization map showing the secondary source responses.

as the wave passed from the bottom of the obstacle toward the top. These decreases in propagation time disappeared after several cycles.

Finally, wavefront shape was also altered during the electric field pulse. As the wavefront propagated across the top of the obstacle, CV decreased significantly at 1 mm from the obstacle edge but not at greater distances in the radial direction, as shown in Fig. 8 *A*. The reduction in CV near the tip caused the wavefront to flatten, as shown in Fig. 8 *B*. At distances >2 mm from the tip the shape of the wavefront was unchanged. The amount of wavefront flattening increased as field intensity increased from 1 to 3 V/cm, and can be seen in Fig. 8 *B* as an advancement of the arm of the wave when the wavefronts are aligned at the tip. At 3 V/cm, the wavefront transiently detached from the top of the obstacle, but remained pinned for the duration of the pulse. Across all experiments, similar results were observed at intensities ≥3 V/cm.

Pulse-break stimulation

At pulse-break, an excitatory response was observed at the obstacle in many of the trials. Fig. 9 *A* shows one such example of pulse-break stimulation. The field stimulus was turned off at $t = 0$ ms, and after some delay ($t = 50$ ms) excitation occurred on the bottom side of the obstacle (hyperpolarized region), opposite to that with pulse-make stimulation (Fig. 1 *A*). Stimulation also occurred at the edge of the monolayer adjacent to the field anode. The incidence

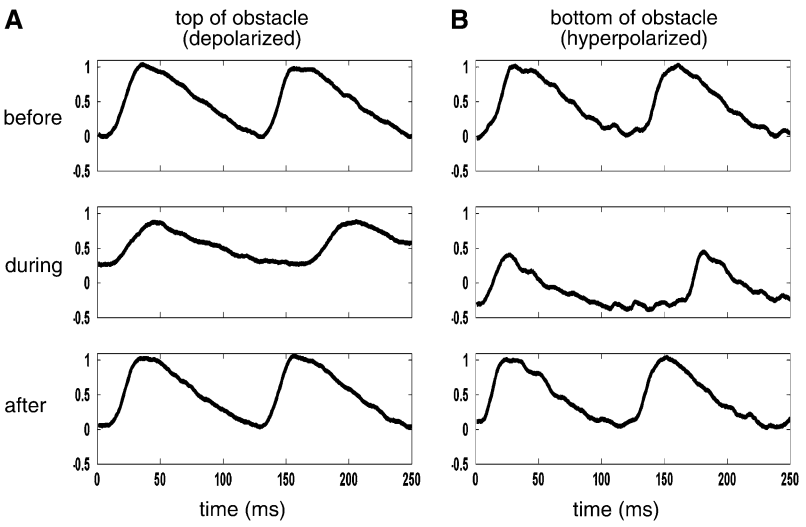

FIGURE 5 Action potential recordings before, during, and after a 3 V/cm electric field pulse of 1-s duration. (*A*) Depolarized region. (*B*) Hyperpolarized region. Action potentials are normalized in amplitude to control action potentials obtained before field stimulation. The upstroke velocity during the pulse normalized to the upstroke velocity before the pulse was 0.66 in the depolarized region and 0.98 in the hyperpolarized region. Wave was pinned to a 3-mm-diameter obstacle.

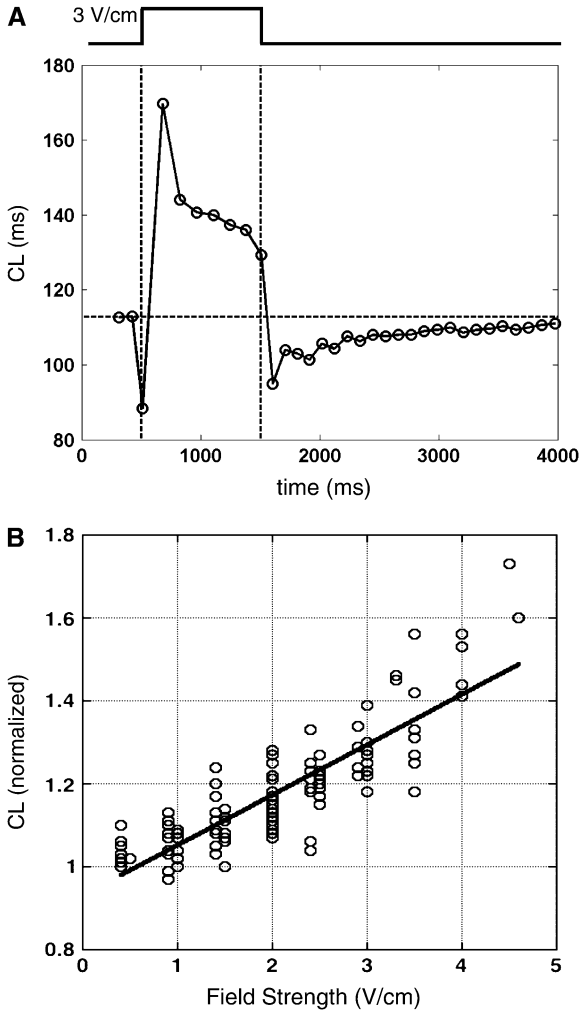

FIGURE 6 Variation in cycle length with time and with field intensity. (*A*) Cycle length (CL) measured before, during, and after 3 V/cm electric field for a wave pinned to a 3-mm-diameter obstacle. CL was measured at a location 2 mm from the top of the obstacle. (*B*) CL during the field pulse versus field strength for all experimental trials. For each trial, CL was averaged during the field pulse and normalized to its value before stimulation. A linear function was fit to the data ($R = 0.86$, $p < 0.005$, $n = 118$).

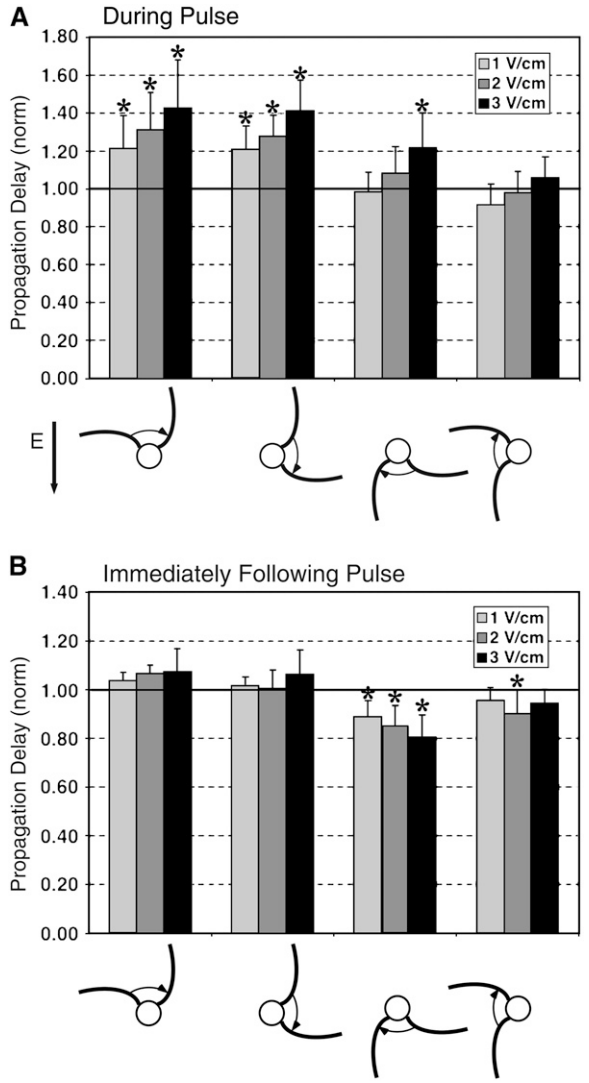

FIGURE 7 Regional propagation delay of a pinned wave around an obstacle. During (*A*) and after (*B*) 1, 2, and 3 V/cm field stimulation. Delay was measured as the wavefront passed through the four 90° quadrants around the obstacle (defined by the angle of the wavefront measured 2 mm from the obstacle), and normalized to the delay before stimulation for each trial. Data are shown such that depolarization (hyperpolarization) is at the top (bottom) of the obstacle. Data is plotted as mean ± SD. Asterisks indicate a mean significantly different than 1 ($p < 0.005$).

of pulse-break stimulation at the obstacle increased with increasing field strength.

Fig. 9 *B* shows an example of pulse-break stimulation that occurred in front of a pinned wave. The 1-s duration, 0.9 V/cm field pulse was turned off at $t = 0$ ms, and at $t = 40$ ms a wave emerged at the bottom side of the obstacle. The excited wave propagated in the antidromic direction and collided with the pinned wave ($t = 60$ ms) causing it to detach ($t = 80$ ms). The detached wave traveled around the refractory region of block, reattached to the obstacle ($t = 110$ ms), and remained pinned for the remainder of the recording.

Detachment due to pulse-break stimulation in the hyperpolarized region at the obstacle was observed in 13 out of 118 trials (11%), and there was one instance of wave termination. The dependence of wave detachment on phase of the wave at the time of pulse-break and on field intensity is shown in Fig. 9 *C*. The depolarized and hyperpolarized regions are at 0° and 180°, respectively (see Fig. 2 *A*). Unlike the case at pulse-make where there was no effect of wave position on detachment success, detachment after pulse-break tended to occur in the hyperpolarized region if the wavefront was passing across the top of the obstacle at the time of pulse-break (−90° to 30°). The mean angle of the wavefront for pulse-break detachment was −19° (0.33 rad) with a concentration, $r = 0.62$, which was significantly different from a circular distribution using the Rayleigh Z test ($p < 0.005$).

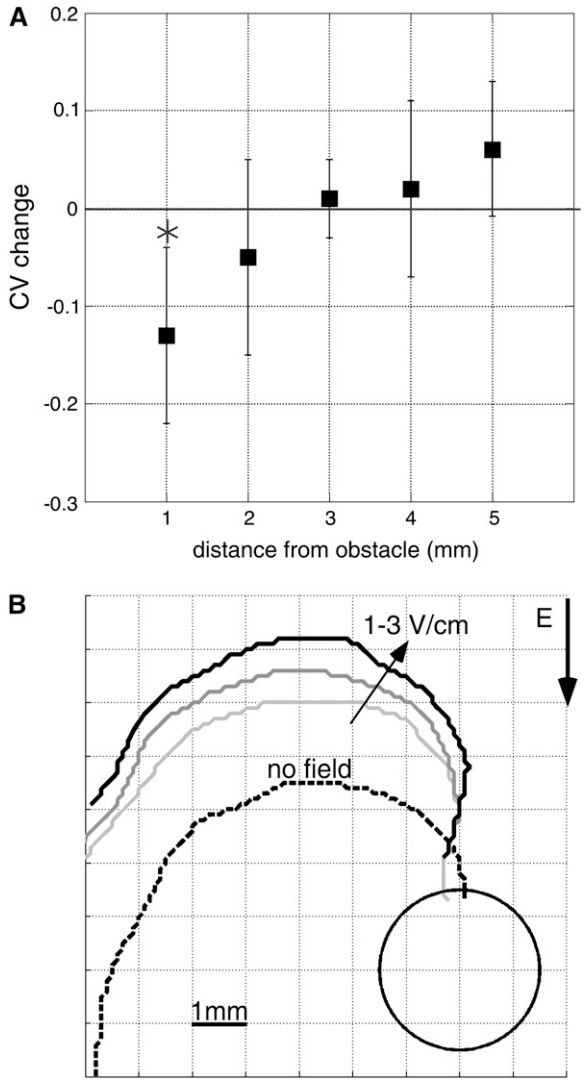

FIGURE 8 Variation in conduction velocity along the wavefront as the wave propagates across the top of the obstacle (region of depolarization). (*A*) Change in CV during 2 V/cm field stimulation at increasing distance from the obstacle edge. CV was measured normal to the wavefront at a point on the wavefront a fixed distance (d) from the obstacle edge measured at $\theta = 0°$. For each trial, CV was averaged during the field stimulus at each location and compared with the average prestimulus CV at the same location. Data is plotted as mean $\pm$ SD. Asterisk indicates a mean significantly different than 1 ($p < 0.005$). (*B*) Wavefront propagation before and during field stimulation at 1, 2, and 3 V/cm for a single experiment. Wavefronts during field stimulation are aligned at a point 1.5 mm from the obstacle edge measured at $\theta = 0°$. During field stimulation, the wavefront flattened near the wave tip, and at 3 V/cm detached from the obstacle.

DISCUSSION

Controlled placement of an obstacle in a homogenous monolayer of cells provides a defined site for wave pinning and excitation during field stimulation. This allows for experimental control comparable with that in numerical models. We have demonstrated that electric field stimulation across a cardiac monolayer interacts in multiple ways with a spiral wave pinned to an obstacle. Secondary sources are formed at the obstacle that can advance or unpin the wave via cathodal make or anodal break stimulation. During prolonged field pulses, depolarization at the obstacle reduces conduction velocity at the tip of the wave, causing an increase in cycle length. Each component of the field pulse may be of potential clinical benefit in stabilizing or terminating reentrant tachycardia.

Pulse-make excitation

Using a numerical model of a cardiac monolayer, Davidenko et al. (6) found that the position and size of the electrodes influence the outcome of pacing interactions with a stationary spiral wave. Larger electrodes placed closer to the core of the wave have a higher probability of affecting the wave. Field stimulation will induce depolarization and hyperpolarization at opposite sides of an unexcitable obstacle (11), allowing for secondary sources of controllable intensity to be placed directly at the tip of a spiral wave that is pinned to the obstacle. The efficacy of defibrillation shock has been attributed to virtual electrode polarization throughout the myocardium providing stimulation sources to terminate fibrillatory activity (16,17).

Woods et al. (18) demonstrated that field stimulation can induce polarization around an insulated cylindrical heterogeneity in isolated rabbit ventricle. The polarization pattern was similar to what we observe in our monolayer preparation. During field stimulation, quiescent tissue is depolarized and excited at the top of the obstacle (Fig. 1 *A*). Stimulation in front of the tip of the pinned spiral wave causes advancement of the wave (Fig. 1, *B–D*). The amount of advancement increases with increasing gap between the wavefront and the stimulation site. Higher intensity stimulation causes the wave to advance into its refractory tail and detach from the obstacle (Fig. 1 *D*). In most cases the wave can propagate around the refractory region and reattach to the obstacle after the tissue has recovered. If reattachment fails to occur, the wave drifts to the boundary of the monolayer and terminates. The ability of the wave to reattach is determined by the pivoting radius of the wavefront and size of the obstacle (19,20). In tissue with reduced excitability, pivoting radius is increased (19) and attachment force is decreased (15). Thus, under these conditions it may be more likely for the wave to detach from the obstacle by a field pulse and terminate at a tissue boundary.

The magnitude of the secondary source at the obstacle increases with hole size (21). This is seen in our preparation by the larger degree of wave slowing for the same stimulus strength for waves pinned to 2.6–4 mm holes compared with 2 mm holes. At the same time the pinning force on the wave will increase with hole size (15,22). Because we found that larger holes require a stronger stimulus to unpin, it appears that the increase in pinning force dominates the ability of the secondary source to unpin the wave.

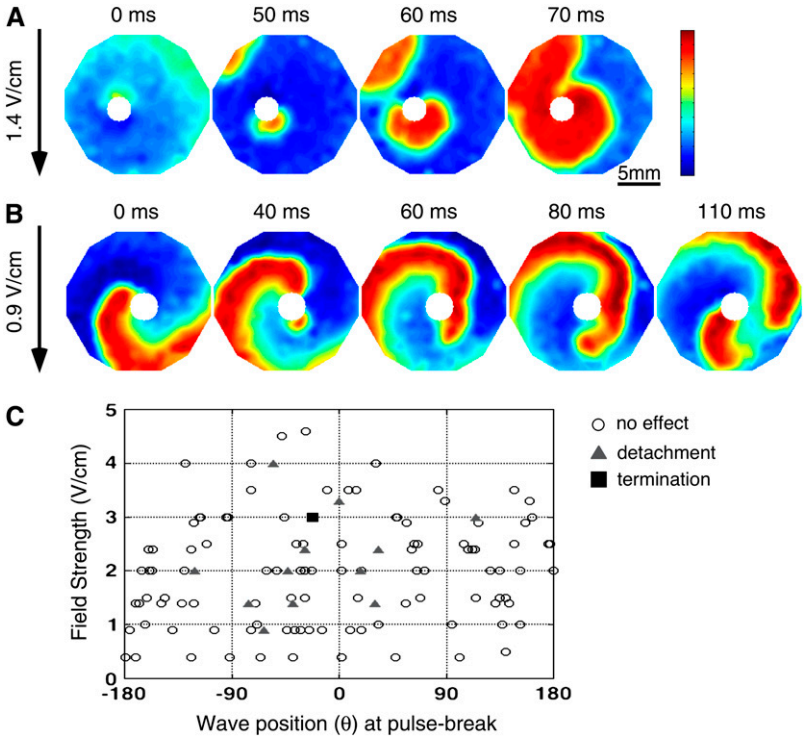

FIGURE 9 Pulse-break stimulation. (*A*) Stimulation of quiescent monolayer containing a 2.6-mm-diameter obstacle. A 1.4 V/cm electric field oriented from top to bottom was applied for 1 s and turned off at $t = 0$ ms. After 50 ms, excited waves appear from regions near the field anode (*upper left edge* of voltage map) and at the obstacle. (*B*) Pulse-break stimulation of a spiral wave pinned to a 3-mm-diameter obstacle in a different monolayer, with a 0.9 V/cm field stimulus turned off at $t = 0$ ms. Stimulation occurred in the region of hyperpolarization causing wave to detach. After stimulation, a new wave was generated that remained pinned to the hole. (*C*) Field strength and timing dependence of wave unpinning. Angle of the wavefront at time of pulse-break is shown. For each experiment, angles were calculated as defined in Fig. 2. The color bar indicates the normalized transmembrane voltage: blue represents the resting state, and red represents the peak of the action potential.

Previous studies using a tissue model of the infarct border zone (12) and a numerical model of excitable media (7) reported a restricted timing window for a field stimulus to detach a pinned spiral wave. This was not the case in our experiments. Detachment depended on the intensity but not the timing of the field pulse (Fig. 2 *B*). At low field intensities we did observe a timing window for maximum advancement of the wave, but unlike previous experimental work in rabbit heart (12) the wave remained pinned to the obstacle. This might be attributed to the smooth circular shape of the obstacle used in our experiments as opposed to native tissue heterogeneities. At higher field intensities we observed secondary sources of excitation at sites other than at the obstacle. Presumably, these sites reflected areas of local micro-inhomogeneities in the monolayer that had little effect during normal wave propagation or at low intensity field stimulation. However, these sites were able to interact with the pinned wave at high field intensities and cause detachment even when the stimulus was applied outside the excitable gap of the wave.

Slowing during the pulse

Long duration electric field stimuli of similar length and intensity similar to our study have been shown to prevent action potential propagation in guinea pig heart (23). We found that action potentials were able to propagate through the regions of polarization at the obstacle, but at significantly reduced velocity. After pulse-make interactions, waves that remain pinned to the obstacle have a cycle length that increases monotonically with field strength (Fig. 6 *B*). The increase in cycle length can be attributed to a reduction in conduction velocity that occurs primarily when the tip of the wave passes through the region of depolarization created by the field on one side of the obstacle (Figs. 7 and 8). The depolarization elevates the resting potential, reduces the upstroke velocity of the action potential (presumably by inducing partial inactivation of the sodium channels), and produces a slowing of conduction that continues for the duration of the pulse (Fig. 5). The amount of slowing varies with distance from the obstacle and field strength. Importantly, our findings demonstrate that the rotational rate of the spiral wave is controlled by the dynamics at the wave tip (the so-called ''rotor'' (24)).

Once the pulse terminates, conduction velocity and cycle length return to their prepulse values. However, the effect is not straightforward or immediate at pulse-break. We observed that many cycles of rotation occur at an accelerated rate before the dynamics return to normal (Fig. 6 *A*). The rate increase occurs predominantly in the region that is hyperpolarized by the field pulse (*bottom side* of the obstacle in Fig. 7 *B*). This suggests that the hyperpolarizing current may have increased sodium channel availability that persists for some time after the current is removed. During the pulse, the increase in sodium channel availability causes an increase in the action potential upstroke velocity that is counteracted by the increased load of the hyperpolarizing current, and therefore, there is no net increase in conduction velocity.

Long-lasting alternating field stimulation has been shown to induce polarization regions that oscillate with the stimulus

and cause a reduction in the defibrillation threshold (25). These alternating secondary sources can produce standing waves of depolarization that halt wave propagation (26). For a pinned wave in our monolayer preparation, alternating electric fields timed such that the wavefront was continuously propagating through depolarized tissue at the obstacle would cause maximum slowing and possibly halt the rotating wave.

Pulse break excitation

A stimulus of sufficient duration can cause anode break excitation in areas of hyperpolarization under a stimulating electrode owing to charge from surrounding depolarized regions diffusing into the hyperpolarized region and triggering excitation (27). In our monolayer preparation, a 1-s-long field pulse was able to excite at the hyperpolarized region at the obstacle via anode break stimulation and cause unpinning (Fig. 9). Anode-break stimulation occurs within the secondary source region of hyperpolarization at the obstacle and not under a physical electrode, but the excitation mechanism is expected to be the same. The delay between pulse-break and visible excitation in the voltage maps (50 ms in Fig. 9 *A*) is longer compared with the excitation delay at pulse-make (10 ms in Fig. 1 *A*) and may be due, in part, to the diffusion of charge providing the excitation trigger.

SUPPLEMENTARY MATERIAL

To view all of the supplemental files associated with this article, visit www.biophysj.org.

We thank Roland Emokpae Jr. for preparing the cell monolayer cultures.

Funding for this work was provided by National Institutes of Health grants No. R01-HL66239 and No. R21-EB006171.

REFERENCES

1. Qu, Z., J. N. Weiss, and A. Garfinkel. 2000. From local to global spatiotemporal chaos in a cardiac tissue model. *Phys. Rev. E Stat. Phys. Plasmas Fluids Relat. Interdiscip. Topics.* 61:727–732.
2. Panfilov, A. V. 1998. Spiral breakup as a model of ventricular fibrillation. *Chaos.* 8:57–64.
3. Gray, R., A. Pertsov, and J. Jalife. 1998. Spatial and temporal organization during cardiac fibrillation. *Nature.* 392:75–78.
4. Tung, L. 1996. Detrimental effects of electrical fields on cardiac muscle. *IEEE Proc.* 84:366–378.
5. Godemann, F., C. Butter, F. Lampe, M. Linden, M. Schlegl, H. Schultheiss, and S. Behrens. 2004. Panic disorders and agoraphobia: side effects of treatment with an implantable cardioverter/defibrillator. *Clin. Cardiol.* 27:321–326.
6. Davidenko, J., R. Salomonsz, A. Pertsov, W. Baxter, and J. Jalife. 1995. Effects of pacing on stationary reentrant activity. Theoretical and experimental study. *Circ. Res.* 77:1166–1179.
7. Takagi, S., A. Pumir, D. Pazó, I. Efimov, V. Nikolski, and V. Krinsky. 2004. Unpinning and removal of a rotating wave in cardiac muscle. *Phys. Rev. Lett.* 93:058101.
8. White, J., G. Walcott, A. Pollard, and R. Ideker. 1998. Myocardial discontinuities: a substrate for producing virtual electrodes that directly excite the myocardium by shocks. *Circulation.* 97:1738–1745.
9. Sobie, E., R. Susil, and L. Tung. 1997. A generalized activating function for predicting virtual electrodes in cardiac tissue. *Biophys. J.* 73:1410–1423.
10. Roth, B., and W. Krassowska. 1998. The induction of reentry in cardiac tissue. the missing link: how electric fields alter transmembrane potential. *Chaos.* 8:204–220.
11. Fast, V., S. Rohr, A. Gillis, and A. Kléber. 1998. Activation of cardiac tissue by extracellular electrical shocks: formation of ''secondary sources'' at intercellular clefts in monolayers of cultured myocytes. *Circ. Res.* 82:375–385.
12. Ripplinger, C., V. Krinsky, V. Nikolski, and I. Efimov. 2006. Mechanisms of unpinning and termination of ventricular tachycardia. *Am. J. Physiol. Heart Circ. Physiol.* 291:H184–H192.
13. Iravanian, S., Y. Nabutovsky, C. Kong, S. Saha, N. Bursac, and L. Tung. 2003. Functional reentry in cultured monolayers of neonatal rat cardiac cells. *Am. J. Physiol. Heart Circ. Physiol.* 285:H449–H456.
14. Entcheva, E., S. Lu, R. Troppman, V. Sharma, and L. Tung. 2000. Contact fluorescence imaging of reentry in monolayers of cultured neonatal rat ventricular myocytes. *J. Cardiovasc. Electrophysiol.* 11: 665–676.
15. Lim, Z., B. Maskara, F. Aguel, T. Emokpae, and L. Tung. 2006. Spiral wave attachment to millimeter-sized obstacles. *Circulation.* 114:2113–2121.
16. Anderson, C., N. Trayanova, and K. Skouibine. 2000. Termination of spiral waves with biphasic shocks: role of virtual electrode polarization. *J. Cardiovasc. Electrophysiol.* 11:1386–1396.
17. Efimov, I., F. Aguel, Y. Cheng, B. Wollenzier, and N. Trayanova. 2000. Virtual electrode polarization in the far field: implications for external defibrillation. *Am. J. Physiol. Heart Circ. Physiol.* 279: H1055–H1070.
18. Woods, M., V. Sidorov, M. Holcomb, D. Beaudoin, B. Roth, and J. Wikswo. 2006. Virtual electrode effects around an artificial heterogeneity during field stimulation of cardiac tissue. *Heart Rhythm.* 3: 751–752.
19. Cabo, C., A. M. Pertsov, J. M. Davidenko, W. T. Baxter, R. A. Gray, and J. Jalife. 1996. Vortex shedding as a precursor of turbulent electrical activity in cardiac muscle. *Biophys. J.* 70:1105–1111.
20. Fast, V. G., and A. G. Kleber. 1997. Role of wavefront curvature in propagation of cardiac impulse. *Cardiovasc. Res.* 33:258–271.
21. Pumir, A., and V. Krinsky. 1999. Unpinning of a rotating wave in cardiac muscle by an electric field. *J. Theor. Biol.* 199:311–319.
22. Pazo, D., L. Kramer, A. Pumir, S. Kanani, I. Efimov, and V. Krinsky. 2004. Pinning force in active media. *Phys. Rev. Lett.* 93:168303.
23. Zhou, X., W. Smith, and R. Ideker. 1997. Prevention of action potentials during extracellular electrical stimulation of long duration. *J. Cardiovasc. Electrophysiol.* 8:779–789.
24. Winfree, A. 1991. Varieties of spiral wave behavior: an experimentalist's approach to the theory of excitable media. *Chaos.* 1:303–334.
25. Meunier, J., J. Eason, and N. Trayanova. 2002. Termination of reentry by a long-lasting ac shock in a slice of canine heart: a computational study. *J. Cardiovasc. Electrophysiol.* 13:1253–1261.
26. Gray, R., O. Mornev, J. Jalife, O. Aslanidi, and A. Pertsov. 2001. Standing excitation waves in the heart induced by strong alternating electric fields. *Phys. Rev. Lett.* 87:168104.
27. Roth, B. J. 1995. A mathematical model of make and break electrical stimulation of cardiac tissue by a unipolar anode or cathode. *IEEE Trans. Biomed. Eng.* 42:1174–1184.